Journal of Hazardous Materials Advances 16 (2024) 100468

Contents lists available at ScienceDirect

Journal of Hazardous Materials Advances

journal homepage: www.elsevier.com/locate/hazadv

$BaTiO_3$ Nanoparticles for highly efficient piezocatalytic reduction of toxic hexavalent chromium: Synthesis, optimization, and kinetic study

Peshawa H. Mahmood [a,b], Omid Amiri [c,d,*], S. Mohammad Sajadi [e]

[a] Scientific Research Centre, Soran University, Soran, Kurdistan-Region, 44008, Iraq
[b] Chemistry Department, College of Science, University of Raparin, Rania, Kurdistan Region, Iraq
[c] Research Center, Cihan University Sulaimaniya, Sulaymaniyah City, 46001, Kurdistan Region, Iraq
[d] Medical Laboratory Analysis Department, College of Health Sciences, Cihan University Sulaimaniya, Sulaymaniyah City, 46001, Kurdistan Region, Iraq
[e] Department of Nutrition, Cihan University-Erbil, KRG, Iraq

ARTICLE INFO

Keywords:
Chromium
Piezo catalysts
Reduction
Kinetic
Thermodynamic

ABSTRACT

Drinking water contamination with heavy metals from industrial activities is an important issue. In particular, the hexavalent chromium ions Cr (VI) which are classified as group (A) carcinogens. Our research reports an effective removal of hexavalent chromium from water through the use of $BaTiO_3$ (BTO) as a piezocatalyst. We meticulously prepared pure tetragonal BTO by optimizing the synthesis parameters. The optimized BTO catalyst was utilized for the removal of Cr(VI) under applied mechanical force and removed up to 96 % of Cr(VI) from the solution. Our kinetic study revealed that the reaction follows a pseudo-first order. Thermodynamic studies indicated that the reaction is most spontaneous at temperatures of 20 °C and concentrations of 20 ppm. Our proposed mechanism for removing Cr(VI) by BTO piezocatalysts suggests that only 15 % of chromium was removed by adsorption, while the rest was removed by reduction through the piezocatalytic process.

1. Introduction

Environmental pollution is a big threat to the health of ecosystems and human populations. It requires serious and comprehensive measures to alleviate its effects (Verma et al., 2023; Kant et al., 2021; Patel et al., 2012). Contamination of drinking water with heavy metals due to industrial activities is one of the most significant issues. In particular, the hexavalent chromium ions Cr (VI) which are classified as group (A) carcinogens (Li et al., 2023). According to the World Health Organisation (WHO), a maximum concentration of 0.05 ppm Cr (VI) is suggested in drinking water (World Health Organization 2020; Vaiopoulou and Gikas, 2020). It poses severe health risks, particularly when it is present in drinking water. It is classified as a human carcinogen due to a strong association with lung cancer from inhalation and possible links to stomach cancer from oral exposure. Mechanistic studies suggest that Cr (VI) can enter cells, causing DNA damage and potentially leading to cancer. While the stomach's acidic environment reduces Cr VI to the less harmful trivalent chromium (Cr III), some Cr (VI) is still absorbed and can cause systemic effects. Animal studies confirm increased cancer risk, particularly stomach tumours, following Cr (VI) ingestion. Therefore, Cr (VI) exposure in drinking water remains a significant public health concern due to its carcinogenic potential (Sedman et al., 2006). Industries that utilize and release Cr (VI) into the environment include leather and textile manufacturing, as well as those involved in electroplating, chemical manufacturing, printing, dyeing, tanning, and metallurgy (Saha et al., 2011; Xia et al., 2019). The feature that makes Cr (VI) more bioavailable and persistent in the natural environment is its high solubility. It is available in different compound forms at different pH. At pH lower than 6.8, it is mostly $HCrO_4^-$ and H_2CrO_4. However, above the pH of 6.8, the most stable form is CrO_4 (Kant et al., 2021; Qiu et al., 2014). In chromate form, Cr (VI) can be reduced to Cr (III) by accepting an electron from the reducing reagent. Cr (III) is also toxic but not as toxic and can be easily removed by increasing the pH to 8 or higher. At this pH, it will become an insoluble form of $Cr(OH)_3$ in water (Chang, 2003).

Different methods have been utilized in the removal of hexavalent chromium ions, such as adsorption (Pakade et al., 2019; Rajapaksha et al., 2022; Owalude and Tella, 2016; Nameni et al., 2008), precipitation (Verma and Balomajumder, 2020; Qin et al., 2005), electrochemical reduction (Chaudhary et al., 2003; El-Taweel et al., 2015;

* Corresponding author at: Research Center, Cihan University Sulaimaniya, Sulaymaniyah City, 46001, Kurdistan Region, Iraq; Medical Laboratory Analysis Department, College of Health Sciences, Cihan University Sulaimaniya, Sulaymaniyah City, 46001, Kurdistan Region, Iraq.
E-mail addresses: peshawa.h.m@gmail.com (P.H. Mahmood), o.amiri1@gmail.com, omid.amiri@sulicihan.edu.krd (O. Amiri).

https://doi.org/10.1016/j.hazadv.2024.100468
Received 7 July 2024; Received in revised form 10 August 2024; Accepted 9 September 2024
Available online 11 September 2024

Lakshmipathiraj et al., 2008; Almaguer-Busso et al., 2009), membrane filtration, ion-exchange (Rengaraj et al., 2001) and biological reduction. Using precipitation methods, Verma et al. reported the reduction of Cr (VI) into its trivalent form Cr (III) by utilising sodium metabisulfite ($Na_2S_2O_5$) and ferrous sulphate ($FeSO_4$) and then precipitated Cr (III) as hydroxide using precipitating agents such as ($Ca(OH)_2$), (NaOH) and a combination of the two. They established that increasing the dosage of sodium metabisulfite from 40 mg/L to 100 mg/L at a pH of 2 increases the % reduction of Cr(VI) from 88 % to 99.97 %. The maximum removal of 98.2 % was achieved by using the combination of $Cr(OH)_2$ and NaOH at a pH of 9[16].

Biological methods encompass a variety of approaches for the removal of Cr (VI). These include integrated bioremediation methods like direct bioreduction and biosorption, as well as additional techniques such as microbial fuel cells, biostimulation, surface-modified dry biomass and biochar adsorption, engineered biofilm, and cell-free reductase processes. These methods utilize a diverse array of living organisms, including bacteria, fungi, plants, leaves, nuts, and algae. Through cellular metabolisms, extracellular activities, physical and chemical adsorption on cell surfaces, and photosynthesis, these organisms effectively transform and eliminate Cr(VI) from water sources (Pradhan et al., 2017).

For the adsorption methods, various adsorbent materials like activated carbon, woody-activated carbons, and biochar have been utilized. The adsorption process also encompasses ion exchange, complexation, precipitation, and electrostatic attraction (Huang et al., 2018; Anah and Astrini, 2017; Yuan et al., 2023). However, most adsorption processes must be conducted in an acidic medium because several studies concluded that the adsorption of Cr(VI) decreases as pH increases towards neutral or basic (Huang et al., 2018; Anah and Astrini, 2017). For example, Rouhaninezhad et al. (2020) studied the effect of pH on the adsorption of Cr (VI) onto micro- and nanoparticles of palygorskite in aqueous solutions and found that as the pH increases, the adsorption diminishes.

Piezoelectric materials, which include ceramics, single crystals, composites, and polymers, have recently been the main topic of research and development (Shaukat et al., 2023). They are functional materials that can transform mechanical energy into electrical energy and vice versa. Mechanical energy is a green and ubiquitous form of energy, that has been used in catalytic reactions (Xie et al., 2023). The piezoelectric material can produce electrons and holes by harvesting energy from mechanical vibrations in the surrounding environment (Amiri et al., 2022). Among the ceramic piezoelectric materials, perovskite oxides have gained a lot of attention. $BaTiO_3$ perovskite is among the first discovered and has been extensively studied for catalytic reactions since it was first reported by Hong et al (Hong et al., 2010).

$BaTiO_3$ (BTO) nanoparticles offer several advantages that make them attractive for piezocatalysis. BTO nanoparticles exhibit high dielectric constants, suitable ferroelectric properties, and piezoelectric characteristics, making them ideal for use in piezocatalysis and piezoelectric devices (Ahamed et al., 2020). It is also environmentally friendly because of its lead-free piezoelectric properties (Lin et al., 2020). Recent studies have demonstrated the potential of piezocatalysts in the simultaneous removal of Cr(VI). For instance, a bifunctional piezocatalyst like Au/BiVO4 has shown significant removal efficiencies for Cr(VI). It has removed 83 % of 10 ppm with piezocatalysis under ultrasonic vibration, indicating that piezocatalysis can enhance the degradation process through the generation of reactive oxygen species (Tu et al., 2020; Wei et al., 2019) Moreover, the integration of piezocatalysis with other techniques, such as photocatalysis, has been explored to further improve the efficiency of Cr(VI) removal from contaminated water (Li et al., 2023; Masekela et al., 2023)

In this study, $BaTiO_3$ has been successfully fabricated through hydrothermal reaction and optimized by changing the hydrothermal temperature (160, 180, and 200 °C) and hydrothermal time (7, 10, and 13 h). It has also been optimized by using different concentrations of precursors while keeping temperature and time constant at 200 °C and 10 h, respectively. Furthermore, the morphological and structural characterizations of the as-prepared catalysts were characterized through X-ray diffraction (XRD), field emission scanning electron microscope (FE-SEM), and transmission electron microscope (TEM), Raman spectroscopy, and BET. The performance of the piezocatalysts was examined by utilizing them for the removal of Cr(VI). The catalyst activity and the active species in the reduction of Cr(VI) were determined along with the reports of the kinetic and thermodynamic studies.

2. Experimental

2.1. Material

Tetraethyl orthotitanate, $BaCl_2{\cdot}2H_2O$ and NaOH were purchased from Sigma-Aldrich company and used as precursor materials without any purification or processing. 1.5 mm diameter Zirconia ceramic balls with a hardness of HRA 87–91 were used to stimulate the piezocatalyst.

2.2. *Synthesis of $BaTiO_3$ nanocatalyst*

2.2.1. Preparation of solutions

To synthesize $BaTiO_3$ piezocatalyst by the hydrothermal method, two solutions were prepared. In the first solution, 5.276 g of $BaCl_2{\cdot}2H_2O$ was dissolved in 20 ml of deionized water until dissolved. Simultaneously, in another experimental set, 10 ml of ethanol was added, followed by the addition of 4.29 g of tetraethyl orthotitanate. it was stirred for a minute before being introduced into the first solution, resulting in the formation of a slurry. Finally, 20 ml of 8 M NaOH was added slowly to the mixture. It should be mentioned that the concentrations were chosen based on a Ba/Ti ratio of 1.6 because several studies prepared tetragonal $BaTiO_3$ successfully using this ratio (Asiaie et al., 1996; Xu et al., 2002; Chen and Chen, 2003).

2.2.2. Hydrothermal synthesis

The resulting solution was poured into the Teflon-lining of a 100-ml sized autoclave at approximately 70 % of its capacity, followed by the immediate closure of the autoclave. The autoclave was then placed in an oven and kept at 200 °C for 10 h. post-incubation, the supernatant was removed, and the precipitate was washed twice with 50 ml of 0.01 acetic acid to get rid of any available $BaCO_3$, and then distilled water was employed to remove any remaining impurities (Wang et al., 2013). Finally, the precipitate was dried at a temperature of 80 °C in an oven.

2.2.3. Optimization of synthesis parameters

To investigate the effects of different synthesis parameters, a series of BaTiO3 catalysts were prepared by varying the hydrothermal temperature, reaction time, and precursor concentrations, as outlined in **Table S1**. These variations included temperatures of 160 °C, 180 °C, and 200 °C, reaction times of 7, 10, and 13 h, and different precursor concentrations.

2.3. Piezocatalytic reduction of Cr(VI)

For the reduction of Cr(VI), 1 g/L $BaTiO_3$ was distributed in a 10 mL Cr(VI) aqueous solution (potassium dichromate solution, $K_2Cr_2O_7$, 20 mg/L) in a 50 ml reagent bottle. To induce piezocatalytic behavior, 5 ZrO_2 balls were added to a narrow-mouth reagent bottle. The solution was slowly stirred in the dark for 30 min to attain adsorption-desorption equilibrium (Amiri et al., 2023). Following, the solution was kept under shaking for 1 h at 350 r/min.

2.3.1. Determination of Cr(VI) concentration

For the determination of Cr(VI), 0.5 ml of the solution was mixed with 0.25 ml of 0.01 M H_2SO_4 and 0.25 ml of 5 ppm of carbazide solution. After incubating for 5 min, the absorbance of the solution was

measured using a UV–visible spectrophotometer at an absorbance spectrum of 543 nm (Lace et al., 2019).

2.3.2. Calculation of Cr(VI) removal rate

The removal rate of Cr(VI) was expressed by the relative variation ratio of time-dependent Cr(VI) concentration described in Eq. (1):

$$\%\ removal = \frac{C_o - C}{C_o} \times\ 100 \quad (1)$$

where C and C_o were the residual and initial Cr(VI) concentrations, respectively.

The effects of catalyst dosage, Cr(VI) concentration, and temperature were studied.

2.3.3. Effect of adsorption

To assess the effect of adsorption on the removal of hexavalent chromium, the nanoparticles were collected, centrifuged, and dried at the end of the experiments. Subsequently, they were added to buffer pH 9 and stirred for 48 h.

2.4. Response surface methodology and statistical analysis

Box and Wilson (1951) introduced response methodology (RSM) with the aim of enhancing production processes within the chemical industry. The primary focus is on optimizing chemical reactions to attain elevated yields and purity while minimizing costs. It relies on polynomial regression modeling for statistical analysis (Nassiri Mahallati, 2020). In this study, the effect of Cr(VI) concentration and temperature (independent variables) on the activity of the piezocatalyst (response) was studied utilizing the Central Composite Design (CCD). CCD is a highly efficient approach offering a sufficient amount of data for the assessment of the model fit without the need for an extensive number of design points, reducing the overall experimental costs (Tarjomannejad et al., 2018).

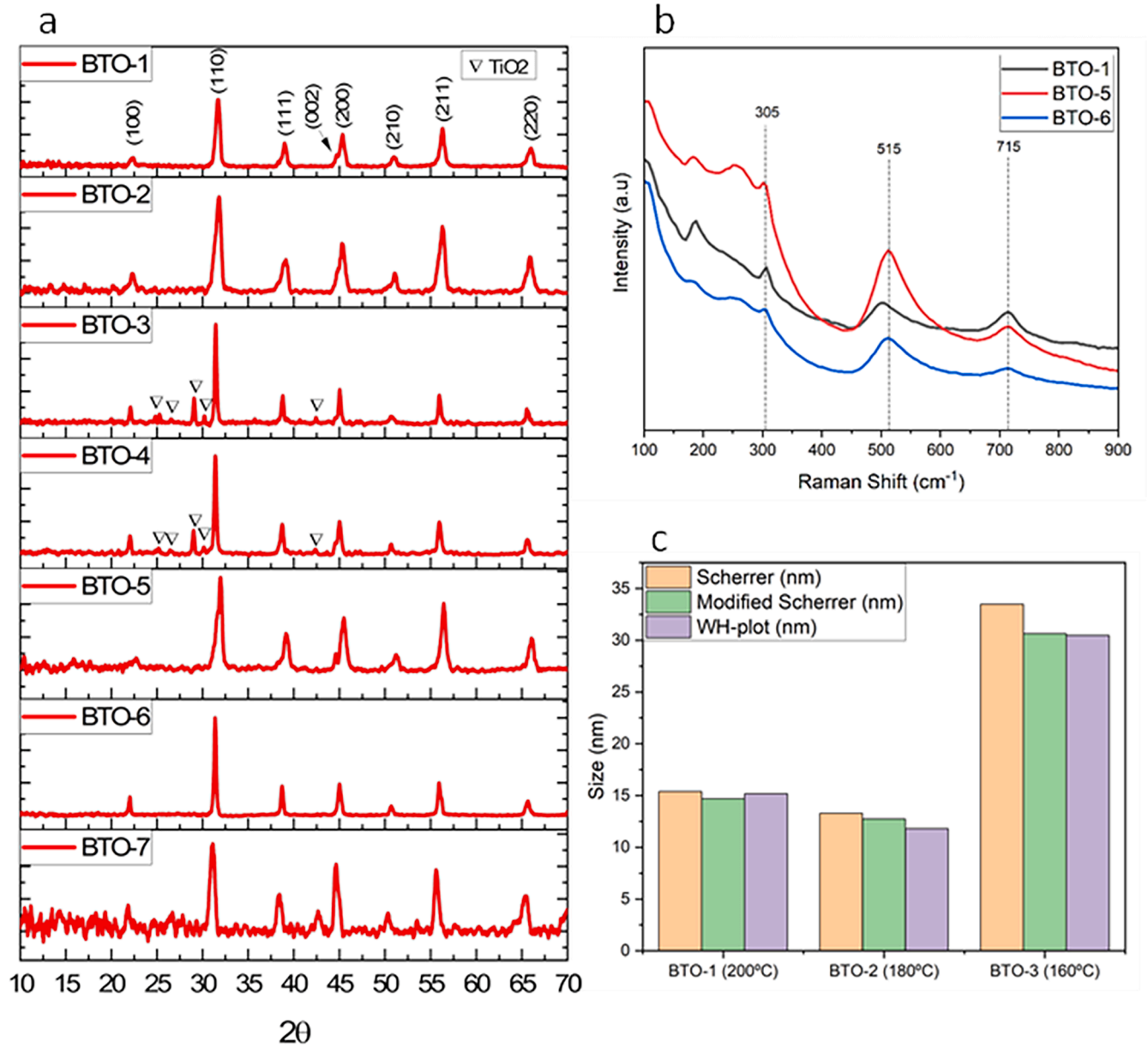

Fig. 1. (a) XRD pattern of samples from BTO-1 to BTO-7. **(b)** Raman spectra of BTO-1 (middle) BTO-5 (above) and BTO-6 (bottom). **(c)** Correlation of different temperature with different methods of determining crystallinity size.

2.5. Studying kinetic and thermodynamics of reaction

The kinetic study of the reaction was performed at a controlled temperature of 20 °C, 40 °C, and 60 °C, for 120 min. At first, samples were collected at short intervals of 1,3,7, and 10 min and then the interval increased to every 5 min. The kinetic studies for piezo reduction reactions were carried out in a batch system with two different concentrations of Cr(VI) (10 and 20 mg/L) at three different temperatures. The pseudo-first-order and pseudo-second-order rate constants were derived by applying non-linear curve fitting methods to the equations representing first-order and second-order reactions. The thermodynamic parameters ΔG, ΔH, and ΔS were calculated using the Von't Hoff equation. The Arrhenius equation was used to determine the activation parameters (Babakr et al., 2022).

3. Results and discussions

3.1. Characterization of as-synthesized piezo catalysts

3.1.1. Structural analysis (XRD & Raman)

The effects of the studied parameters, such as temperature, time, and concentration of precursors, were monitored by X-ray Powder Diffraction (XRD). The characterizations were conducted using a PANanalytical X'Pert PRO, scanning at 1°/min across a 2θ range of 10° to 70°, with Cu Kα radiation (λ = 1.5406 Å) as shown in Fig. 1 a. The peaks at 2θ: 22.27, 31.75, 39.04, 44.64, 45.40, 51.03, 56.30, and 65.97° were assigned to (100), (110), (111), (002), (200), (210), (211), and (220) in support of the perovskite phase of barium titanate for all the samples. The average crystallite size was calculated using three different methods: the Scherrer equation, the modified Scherrer equation, and the William Hall method. Crystallinity was calculated using the method reported by (Khan et al. (2019), Navarro-Pardo et al. (2013). The results of the calculations are summarized and listed in **Table S2**.

Raman spectroscopy was carried out on a TEKSAN tekram using a laser with a wavelength of 532 nm. Raman spectroscopy can be utilized for the $BaTiO_3$ samples to further determining the phases (tetragonal or cubic) and crystallinity. The tetragonal phase of $BaTiO_3$ displays characteristic peaks located at 301 and 715 cm^{-1}, which are attributed to the B1 + E(TO_3 + LO_2) and A1 + E(LO_3 + LO_4) phonon modes responsible for Ti−O torsional vibration in the TiO octahedral. The measured peak located at 507 cm^{-1} is attributed to TO_3 of the A1 symmetry (Kalhori et al., 2023; Hayashi et al., 2013). Fig. 1 b. shows the Raman spectra of BTO-1, BTO-5, and BTO-6. The bands around 515 cm^{-1} are seen in all the samples. The peaks around 305 and 715 cm^{-1} which are characteristic of the tetragonal $BaTiO_3$ phase, are sharp in BTO-1 and BTO-5, reduce their sharpness, and become indistinct in BTO-6, indicating its cubic phase (Kalhori et al., 2023; Hayashi et al., 2013).

3.1.2. Morphological analysis (SEM, EDS & TEM)

To understand the effect of hydrothermal time, temperature, and concentration of precursors on the morphology, size distribution, and surface roughness of prepared $BaTiO_3$, field emission scanning electron microscopy (FE-SEM) and EDS were utilized for all samples. The results for all samples are shown in **Fig. S1.**

Energy Dispersive Spectroscopy (EDS) was used for determining the elemental analysis of the synthesized piezocatalytic nanoparticles. **Fig. S2** shows the spectrum for all the samples.

Transmission Electron microscope (TEM) was used for characterization of the BTO-1 nanoparticles, as it has been used in the study of piezo reduction of hexavalent chromium Cr(VI). The associated particle size distributions were derived from the analysis of the images from TEM, and are shown in Fig. 2.

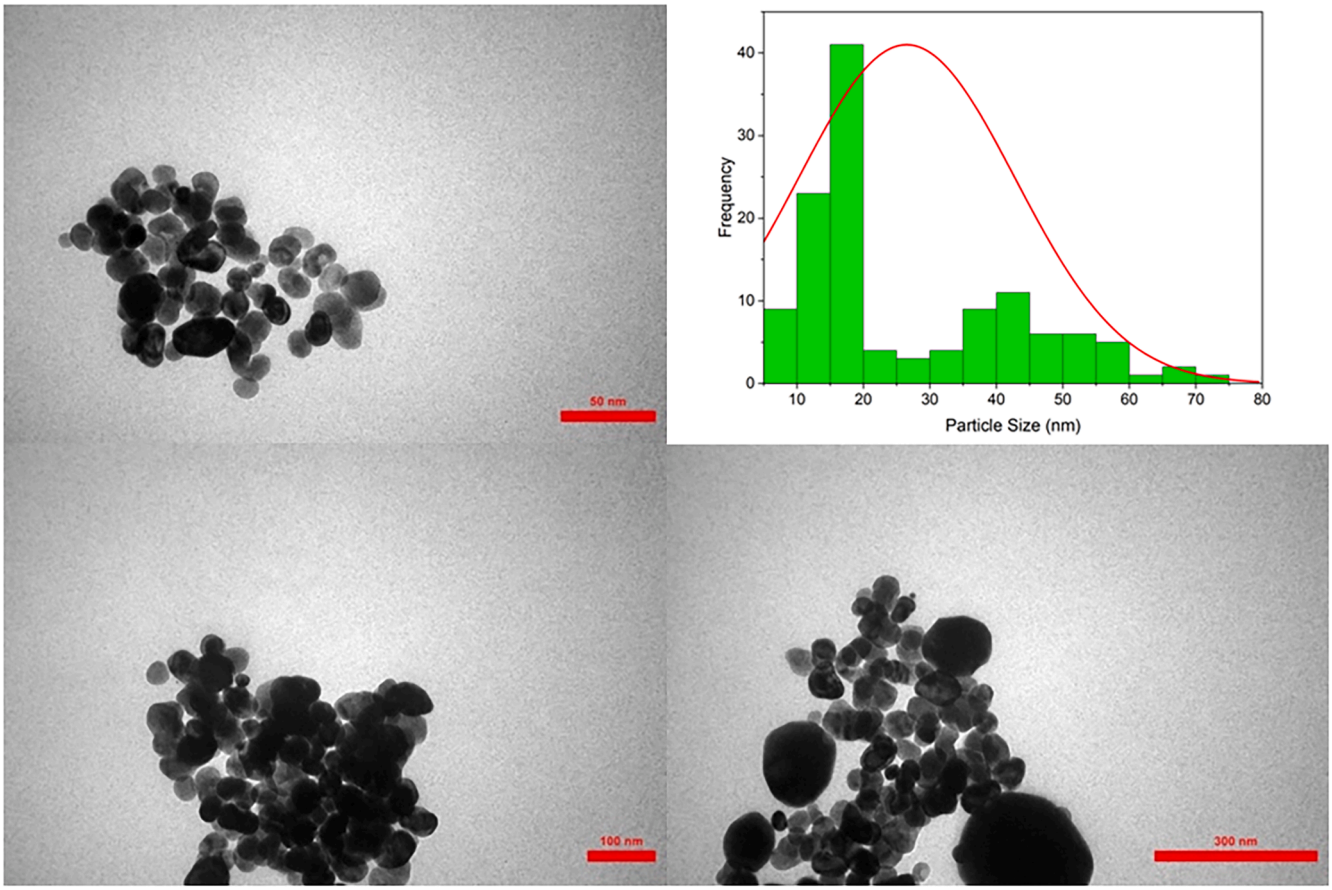

Fig. 2. TEM of BTO-1 and particle distribution derived from analysis of the images.

3.1.3. BET characterization

BET (Brunauer-Emmett-Teller) characterization is a widely used method for measuring the specific surface area of materials. The technique is based on the physical adsorption of gas molecules onto a solid surface to determine the surface area of the sample (Brunauer et al., 1938).

BET was used to find the correlation between the surface area and the removal capacity of the synthesized nanoparticles. Four samples (BTO-1, BTO-5, BTO-6, BTO-7) were chosen based on their removal capacity of Cr(VI). Fig. 3 shows the correlation between the % Removal and surface area. **Fig. S3** shows the adsorption/desorption isotherms and BET isotherms of the four samples.

3.1.4. Effect of hydrothermal temperature

It has been found that the hydrothermal temperature has a significant effect on the prepared $BaTiO_3$[51]. Our results show, at hydrothermal temperature of 200 °C, the synthesized $BaTiO_3$ was primarily tetragonal phase, which is in agreement with Maxim et al. (Maxim et al., 2008) They have prepared $BaTiO_3$ with a different precursor within 24 h. The crystal phase was tetragonal at 200 °C. It can be seen from the indexed data, (c/a) ratio is equal to 1.009. As shown in Fig. 1 c, by lowering the hydrothermal temperature from 200 °C to 180 °C, the average sample crystalline size was slightly lowered. However, the tetragonality of the sample decreased as (c/a) became 1.006. This aligned with the report of Cifti et al. (Ciftif) who reported that at lower temperatures the crystalline size decreases. In contrast, at a temperature of 160 °C, the crystal structure changed from tetragonal to cubic (c/a = 1). As denoted by the disappearance of the secondary split, it appears around ~ 45° which corresponds to (200) and (002) diffraction peaks in tetragonal phase. As the temperature decreased to 160 °C, the traces of impurity appeared as TiO_2 and $BaCO_3$. Which indicates the non-completion of the reaction. The calculated average size of nanoparticles became larger, as shown in **Table S2** and Fig. 1 c. which may be due to the integration of TiO_2 and $BaCO_3$ in the crystal structure of $BaTiO_3$ (Uchino et al., 1989).

In Fig. 2 the particle shapes were found to be oval-shaped and quasi-spherical particles. The particle size distribution reported that most of the particles were 14 nm in size. The crystalline size of BTO-1 using Scherrer, modified Scherrer, and WH Plot was 15.39, 16.69, and 15.17 nm, respectively. Most particle sizes are around 17.5 nm, and the normal distribution was 26.52 nm.

As shown in **Fig. S1**. The SEM images exhibited that at 200 °C the particles were egg-shaped and there was a noticeable agglomeration, as indicated by the results of BET by low surface area. The surface of the particles was rough and granular, indicating the presence of smaller nanoparticles attached to the larger ones. As the temperature decreased to 180 °C, the particles became more uniform and less agglomerated. The surface of the particles has also become smoother. At a lower temperature of 160 °C, the particle sizes become more irregular and more compact, and agglomeration becomes quite pronounced. It seems that the morphology change was due to the presence of the impurities (TiO_2 and $BaCO_3$) (Shiomi, 2023).

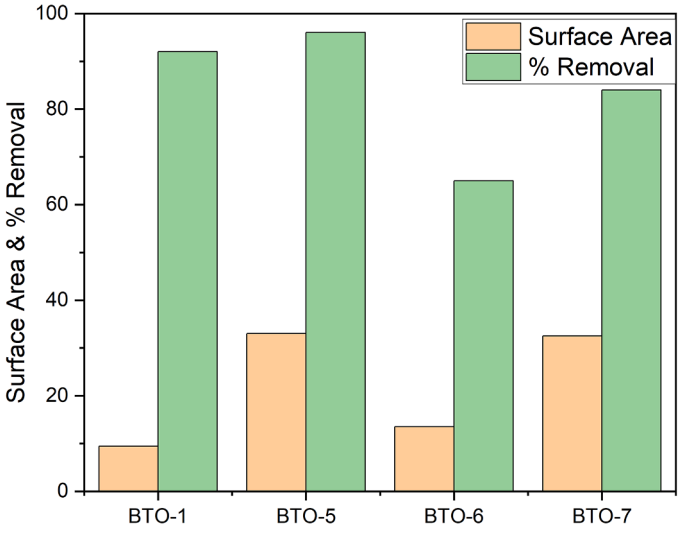

Fig. 3. Correlation between surface area and % removal.

3.1.5. Effect of reaction time

The effect of reaction time under hydrothermal conditions was studied at three different times (7, 10, and 13) hours at a temperature of 200 °C. The results reported that, at a shorter time of 7 h, the prepared nanoparticles exhibited the same phase and indexing of $BaTiO_3$ at 160 °C and 10 h, which is primarily cubic and contains TiO_2 and $BaCO_3$ impurities as seen in Fig. 1 **a**. For a longer time 10 h, the tetragonality increases, and (c/a) ratio is equal to 1.009. Under a 13-hour reaction time, the tetragonality decreases (c/a = 1.007). The size of the particles also became smaller. When the size of the crystallites measured using Scherrer, modified Scherrer and Williamson Hall plot methods, it was found that as the incubation time increases the crystallite sizes decrease. For 7 h were 23.39 nm, 24.11 nm, and 36.29 nm, 10 were 15.39 nm,14.69 nm, and 15.17 nm, and 13 h were 14.31 nm, 9.84 nm, and 6.11 nm, respectively. To better understand this phenomenon, stain in these three crystallites were calculated using Williamson Hall plot. The strain values were 0.00155, 0.0001180, and -0.00694 from shortest to longest incubation time. Increasing strain from tensile to lower tensile, eventually to compressive inside the crystallites indicate that as the incubation time increases the compression on the crystals increase and lead to smaller crystallites. Motevalizadeh et al (Motevalizadeh et al., 2014). reported similar trend when synthesizing ZnO using hydrothermal method.

The effect of hydrothermal time on particle morphology, size, and shape was studied using FE-SEM. At a reaction time of 7 h (BTO-4), the particles were more spherical and uniform but had a distinctly rough surface texture. The agglomeration is quite high. At 10 h of reaction time (BTO-1), the particles were also uniform in size. with a smoother surface texture. As the time increased to 13 h (BTO-5). The particles became relatively spherical with a moderately rough and granular surface texture. The surface area was increased compared to BTO-1 according to BET as shown in Fig. 3.

3.1.6. Effect of precursor concentration

Three different precursor concentrations (BTO-1, BTO-6, BTO-7) inside the autoclave were studied at a temperature of 200 °C and for 10 h of incubation, as shown in **Table S1**. In the case of BTO-7, which has the lowest concentration, the XRD pattern depicted a very noisy pattern. When the calculation for determining the crystallinity was performed, it was found to be the lowest among the samples, at only 55 %. Additionally, impurities such as TiO_2 were detected in the sample. The patterns correspond closely to JCPDS No. (98-002-9787) which has a cubic phase. When the concentration doubled from (BTO-7) to (BTO-6), a perfect cubic structure was synthesized which was closely related to pattern index JCPDS No. (98-016-6225). The crystal size was larger, and crystallinity was very high, at around 87 %.

At a lower precursor concentration (BTO-7), SEM images exhibited highly aggregated particles, which might be because of their low crystallinity and quite complex morphology. However, as concentration doubled (BTO-6), the morphology of the particles depicted a mixture of spherical and irregular-shaped particles, which became smaller but with a varied particle size distribution.

3.2. Piezo catalytic activity

The mechanism of the piezocatalyst, triggered by the mechanical energy resulting from the impact of zirconia balls, is shown in reactions (2) to (5). The equations exhibited the formation of electrons and holes

from opposite sides of the perovskite $BaTiO_3$. These species serve as anodic and cathodic interfaces for chemical degradation or reduction of pollutants. In the absence of other materials, these electrons and holes react to make hydroxy radicals and superoxide radicals.

$$BaTiO_3 + \text{Mechanical energy} \rightarrow BaTiO_3\ (e^- + h^+) \quad (2)$$

$$e^- + O_2 \rightarrow O_2^{\bullet} \quad (3)$$

$$O_2^{\bullet} + Cr^{6+} \rightarrow Cr^{3+} \quad (4)$$

$$h^+ + H_2O \rightarrow {}^{\bullet}OH + H^+ \quad (5)$$

At first, the catalytic activity of prepared $BaTiO_3$ was evaluated in the removal of Cr(VI). Fig. 4 a. The % removal for both BTO-1 and BTO-2 was 92 %, which increased to 95 % for BTO-3. The highest removal percentage was found in the case of BTO-4 and BTO-5 (95 %). However, the lowest removal percentage was found in BTO-6, which was 65 %, followed by BTO-7.

3.2.1. The effect of catalyst dosage

The effect of catalyst dosage on piezocatalytic activity is represented in Fig. 4 b. It was reported that the result of % removal did not significantly increase the reduction of Cr(VI) solution with increased catalyst dosage. The degradation (reduction) efficiency of 10 ppm Cr(VI) at 1, 3, 5, and 7 g/L of the $BaTiO_3$ concentration was determined to be 87.53 %, 88.31 %, 88.77 % and 89.42 % respectively. In addition, increased concentrations of the catalyst increased the reduction efficiency of the solution very slowly due to the agglomeration of nanoparticles (Ismael et al., 2022). It can also be attributed to the fact that when the dosage increases, it results in more active sites. However, the force required to activate the piezocatalyst remains constant. Consequently, with more nanoparticles present, the force exerted per nanoparticle decreases. In this study, the amount of $BaTiO_3$ (1 g/L) was favored at the industrial scale to avoid the risk of the nanomaterials as secondary contamination (Table 1).

3.2.2. The optimization of temperature and concentration

The response surface modeling (RSM) was utilized with central composite design to model the removal conditions of Cr(VI) by $BaTiO_3$ (BTO-1). The effect of temperature and concentration of Cr(VI) was investigated. A total of 15 experiments were run in three different trials. The average values were added to the response part. **Table S1** consists of a summary of the experiments and their corresponding experimental and predictive results. Polynomial equations were computed using experimental data to predict the response variable values. The equation derived from response surface methodology for the response variable is shown in Eq. (6):

$$Y = 105 - 2.60X_1 + 0.29X_2 - 0.1534X_1 * X_1 - 0.00163X_2 * X_2 + 0.02704X_1 * X_2 \quad (6)$$

where Y, X_1, and X_2 are the % Removal (response), concentration of Cr (VI) and temperature of the reaction, respectively.

Based on the results, the regression coefficient values and their corresponding t-values and p-values are listed in Table 2. The corresponding p-value < 0.500 indicated the significance of the model term. The temperature * temperature term is the only term with a p-value of 0.782, denoting its non-significance. The model fits the experimental data with an R^2 of 93 % and an R^2 (Pred.) of 77.44 %. The response was highly significant (p 0.05) based on the results. The large T-values and p-values < 0.05 indicate that the model can explain variations in the

Table 1
Summary of experiments and their corresponding results.

Run	Concentrations (ppm)	Temperature (K)	Removal (Exp.) (%)	Removal (Pred.) (%)
1	5	293	73.28	71.3570
2	5	313	58.32	60.0080
3	5	333	41.81	47.3530
4	10	293	87.32	86.4725
5	10	313	82.06	77.8280
6	10	333	75.39	67.8775
7	15	293	89.99	93.9180
8	15	313	85.50	87.9780
9	15	333	81.21	80.7320
10	20	293	91.23	93.6935
11	20	313	89.64	90.4580
12	20	333	84.51	85.9165
13	25	293	89.42	85.7990
14	25	313	86.02	85.2680
15	25	333	82.39	83.4310

Table 2
Regression coefficient values and their corresponding T-value and P-values.

Term	Coef	SE Coef	T-Value	P-Value
Constant	87.98	2.27	38.69	0.000
Concentration	12.63	1.53	8.27	0.000
Temperature	-6.59	1.32	-4.98	0.001
Concentration*Concentration	-15.34	2.58	-5.94	0.000
Temperature*Temperature	-0.65	2.29	-0.28	0.782
Concentration*Temperature	5.41	1.87	2.89	0.018

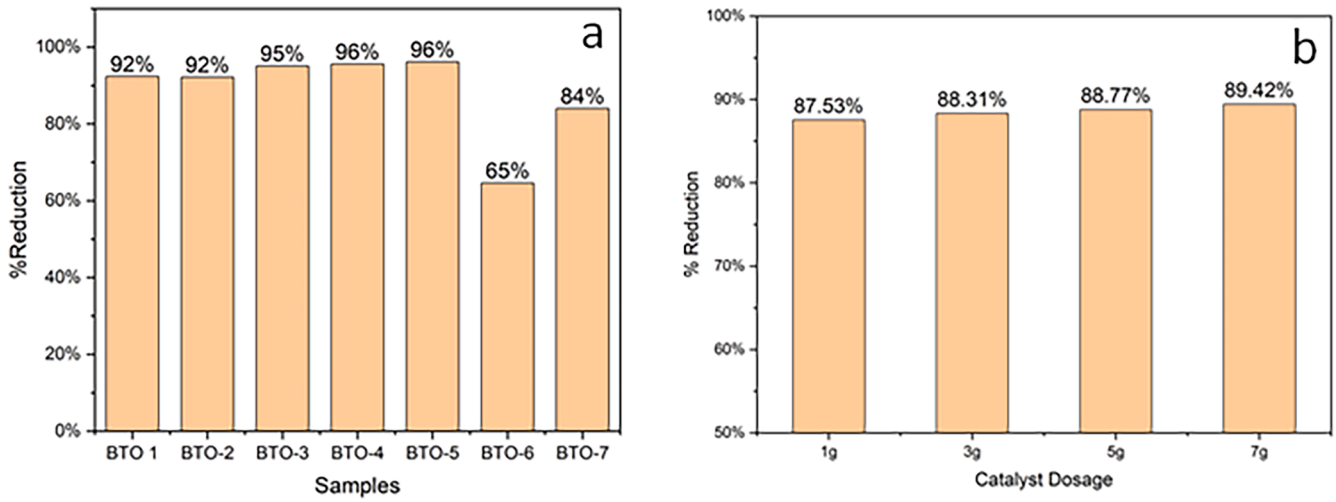

Fig. 4. (a) $BaTiO_3$ assessment for removal of Cr(VI). **(b)** Catalyst dosage of 1, 3, 5, 7 g BaTiO3 for reduction of Cr(VI).

responses.

Fig. 5 a and b show a three-dimensional response surface and contour plot to determine the removal percentage of Cr(VI) over the different temperatures of the solution and concentration of Cr(VI). Fig. 5 c displays the Pareto analysis that corresponds to the degradation (Reduction) of Cr(VI). Both independent variables (concentration and temperature) have made significant contributions, as confirmed by the Pareto analysis results. The removal percent was more affected by the effect of concentration. Fig. 5 d is the comparison of experimental data and calculated values for the response, exhibiting a very good agreement of predicted value with the experimental data by the model.

The results suggest that the reduction ability of the piezocatalyst is affected by the temperature and concentration of the solution. The optimum values for the highest removal of hexavalent chromium of 94.76 % are 17.32 ppm and 20 °C for concentration and temperature, respectively. The results align with the Babakr et al. (2022) study, which studied the effect of temperature on the peizocatalytic efficiency of nanoparticles and concluded that as temperature increases, the piezocatalytic activity decreases. According to the results of the experiment, as the initial concentration of chromium (VI) increases, the percentage removal decreases, which indicates that the effect is in fact, the reduction of chromium (VI) rather than adsorption. According to adsorption studies, Gupta et al. (2016) found that when the initial concentration increased, the removal of hexavalent chromium increased. Yuan et al. (2023) also reviewed the removal of hexavalent chromium Cr(VI) in aqueous solutions using polymeric materials. They state that the adsorption of Cr(VI) is an endothermic process. Increasing the reaction temperature can enhance the adsorption of Cr(VI).

3.2.3. Adsorption and desorption test

Studies have found that Cr(VI) is better desorbed at higher pH (Anah and Astrini, 2017; Jadidi et al., 2017). To assess the impact of adsorption on the removal of Cr(VI) by the piezocatalyts, 1 g/L of the catalyst was added to a solution of 20 ppm Cr(VI) and shaken at 350 r/min with 5 zirconia balls. Consequently, the nanoparticles were centrifuged and dried in the oven at 80 °C. The dried particles were reused in buffer pH 9 to desorb the adsorbed chromium ions. Then, the nanoparticles were stirred with magnetic bars for 48 h. The results of the experiment shown in Fig. 6 a reported that only 15 % of Cr(VI) was desorbed, indicative of the fact that 85 % of chromium is reduced.

3.2.4. Scavenger test

Scavengers play an important role in understanding the mechanism of the peizocatalytic process by selectively quenching or reacting with specific reactive species. Their application is instrumental in identifying the primary reactive species responsible for the piezocatalytic reaction (Ismael et al., 2022; Amiri et al., 2021; Ahmed et al., 2023). When mechanical stress is applied to a piezocatalyst, it generates electron-hole pairs. These charge carriers migrate to the surface, initiating redox reactions with the materials present. It is known that they generate reactive oxygen species (ROS), superoxide anions ($O^{-2}\bullet$) and hydroxyl radicals (•OH) through reactions with dissolved oxygen and water (Xie et al., 2023; Babakr et al., 2022).

In this study, benzoquinone, isopropanol, and methanol are employed as scavengers for superoxide radicals, hydroxy radicals, and holes, respectively. As shown in Fig. 6 b, the reduction efficiency was 89.8 % in the absence of scavengers. However, the addition of benzoquinone further reduced the reduction efficiency to 72.85 %. This observation is consistent with previous studies that suggested the

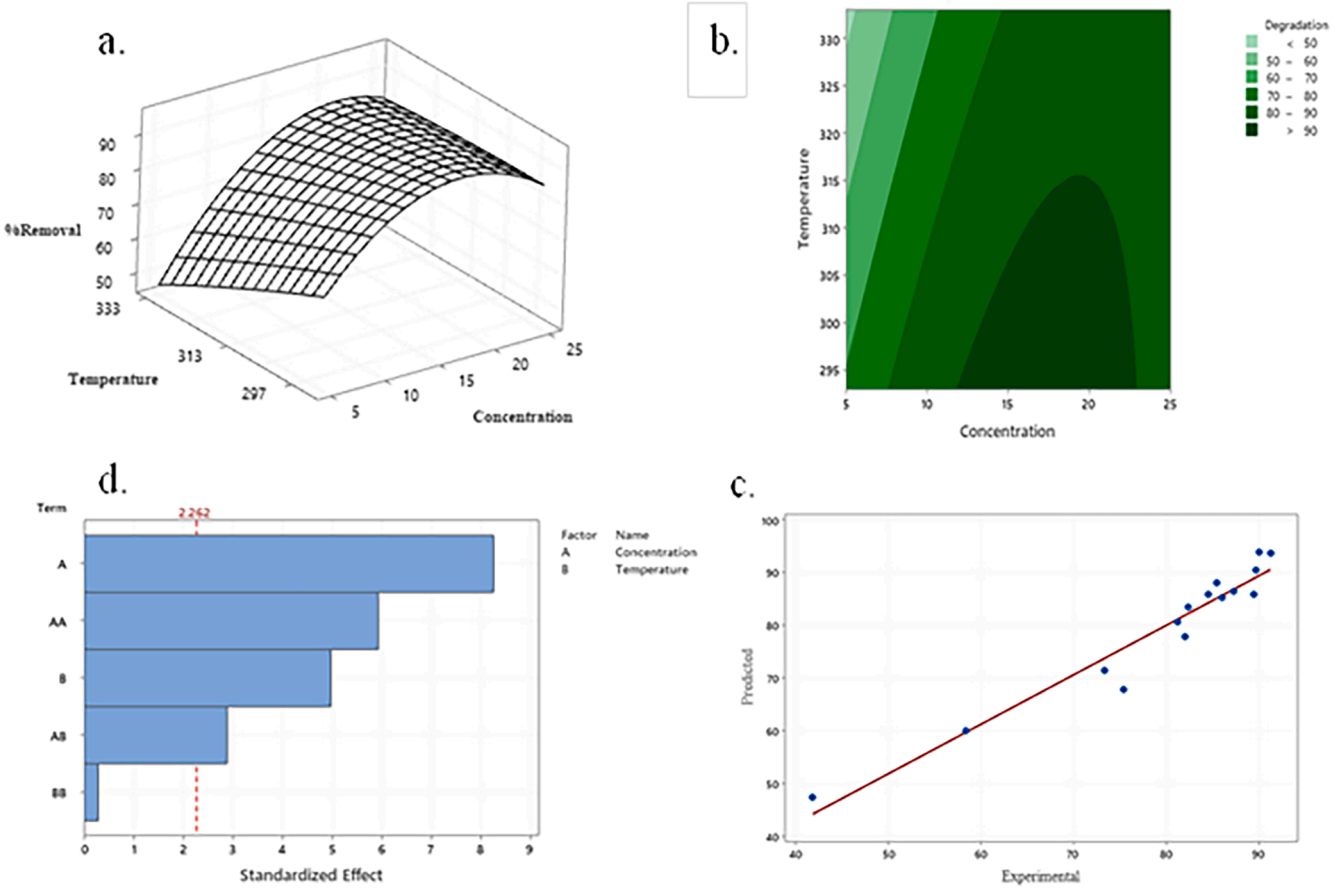

Fig. 5. **(a)** 3D surface plot of % removal of Cr(VI) vs Temperature and concentration. **(b)** Contour plot of % removal vs Temperature and concentration. **(c)** Pareto chart of the standardized Effects, the response being % removal. **(d)** Response surface methodology of predicted vs Experimental.

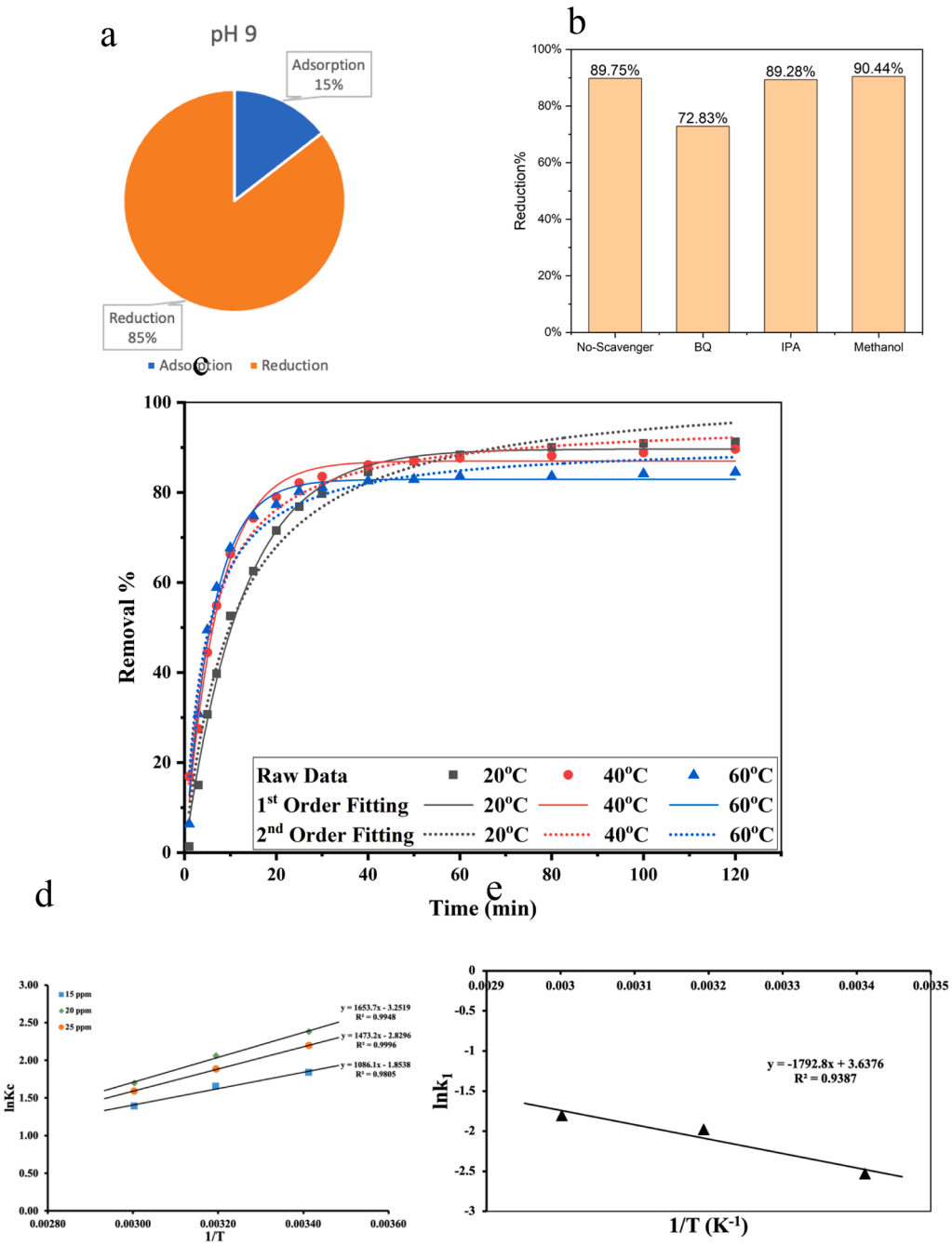

Fig. 6. (a) Adsorption and Reduction percentage of Cr(VI). **(b)** Using Scavengers Benzoquinone, Isopropanol and methanol. **(c)** pseudo-first-order and pseudo-second-order models in different temperatures. **(d)** Graph between $\ln K_c$ (equilibrium constant) and 1/T **(e)** Graph between $\ln k_1$ (rate constant) and 1/T for calculation of activation energy.

reduction reaction is primarily driven by superoxide radicals (Djellabi et al., 2022; Deng et al., 2017). Conversely, when only methanol, a hole scavenger, was introduced, the reduction efficiency increased to 91.2 %. This indicates that the addition of a hole scavenger delayed the saturation of the peizocatalyst, thereby enhancing its activity. The addition of isopropanol did not change the reduction efficiency, which suggests that hydroxy radicals do not participate in the reduction reaction of hexavalent chromium.

3.2.5. *Kinetic and thermodynamic study*

The reduction reaction and its characteristic constants can be studied through pseudo-first-order, pseudo-second-order, and intra-particle diffusion to study kinetic measurements. Lagergren's developed non-linear pseudo-first order model and it is as follows (Moussout et al., 2018):

$$q_t = q_e\left(1 - e^{-k_1 t}\right) \tag{7}$$

where q_t and q_e (mg/g) are the amounts of the Cr(VI) reduced at time t (sec) and at equilibrium, $k_1(\text{min}^{-1})$ is the rate constant. Lagergren's pseudo-second-order kinetic model assumes that the rate of degradation is second order.

$$q_t = \frac{q_e^2\, k_2\, t}{1 - (q_e\, k_2\, t)} \tag{8}$$

where k_2 is the pseudo-second-order rate constant.

Table 3 summarizes the kinetic parameters for both pseudo-first-order and pseudo-second-order models at different temperatures (20, 40, and 60 °C) at a shaker speed of 253 r/min which were obtained from non-linear regression of the isotherm models.

The pseudo-first-order model is a better fit to the experimental data for the reaction, as R^2 is 0.993, 0.99, and 0.989 for temperatures of 20, 40, and 60 °C, respectively. However, R^2 of the pseudo-second-order model is lower, which is 0.981, 0.983, and 0.964 for the same temperatures.

The pseudo-first-order model is characterized by the parameters q_m (maximum reduction percent), K_1 (the rate constant), and R^2. The value of q_m decreases with increasing temperature, from 89.65 % at 20 °C to 82.91 % at 60 °C, indicating a slight decrease in reduction capacity at higher temperatures. The rate constant K_1 shows an increasing trend with temperature, from 0.079 to 0.138 and further to 0.165 for 20, 40, and 60 °C, respectively. suggesting enhanced kinetics at higher temperatures. Both kinetic models are shown in Fig. 6 c.

The pseudo-second-order model shows a similar pattern as the aforementioned model; q_m value also decreases with increasing temperature, and the rate constant also increases. The results indicate that the reduction capacity decreases and the rate constant increases with rising temperature, indicating that while the reduction of Cr(IV) is somewhat less efficient at higher temperatures, it proceeds more rapidly.

It has been found that polarization and piezoelectric coefficient of ferroelectrics are impacted by temperature in a significant way (Kalhori et al., 2023). Studies found that $BaTiO_3$ has a spontaneous polarization of 0.26 C m^{-2} at room temperature, which decreases to 0.22 C m^{-2} at about 80 °C and continues to decrease with increasing temperature (Meng et al., 2023). As the temperature approaches the Curie temperature Tc of $BaTiO_3$ (120 °C), the nanocatalyst undergoes a ferroelectric to paraelectric phase transition. During this transition, $BaTiO_3$ shifts from a polar tetragonal phase to a non-polar cubic phase. Consequently, the spontaneous polarization and the piezoelectric coefficient diminish and eventually reach zero. Our results also align with those of Amiri et al who found that as temperature increases, the peizocatalytic behavior of $BaTiO_3$ decreases (Amiri et al., 2022).

The thermodynamic parameters for the piezo reduction of Cr(VI) by $BaTiO_3$ nanoparticles are summarized in Table 4 . The value of ΔH is the enthalpy change (kJ mol^{-1}), ΔS is the entropy change (kJ mol^{-1} K^{-1}), and ΔG is the free energy change (kJ mol^{-1}) for each initial concentration of (15, 20, 25 ppm) presented. The Von't Hoff equation was used for calculating the thermodynamic parameters (ΔG, ΔH, and ΔS).

It can be seen from Table 4 that the Gibbs free energy (ΔG) values were negative at all temperatures, which indicated that the reactions were spontaneous under the conditions studied. Notably, ΔG of the initial concentration of 20 ppm at 20 °C is −5.82 kJ mol^{-1} which is the most negative among the values observed. This implies that under these specific conditions, the reaction is more thermodynamically favorable and proceeds more readily compared to other conditions. The negative values of ΔH indicate that the reduction of Cr(VI) by $BaTiO_3$ nanoparticles is exothermic. The negative value of ΔS suggests a decrease in disorder during the reduction process. Comparison of the finding of this study compared to other studies is summarized in Table 5

Fig. 6 e shows the activation energy of the reaction using the Arrhenius equation which, is 14.90 kJ mol^{-1}. It suggests that the reduction proceeds at a significant rate, even at relatively low temperatures.

Table 3
Summary of kinetic parameters for both pseudo-first-order and pseudo-second-order models at different reaction temperatures.

Kinetic Models	Parameters	Different Temperature		
		293 K	313 K	333 K
Pseudo First Order	q_m	89.65	87.00	82.91
	K_1	0.079	0.138	0.165
	R (Kant et al., 2021)	0.993	0.9904	0.98985
Pseudo Second Order	q_m	103.93	96.23	91.05
	K_2	0.0009	0.00197	0.0025
	R (Kant et al., 2021)	0.981	0.983	0.964

Table 4
Thermodynamic parameters for the reduction of Cr(VI) using $BaTiO_3$.

Initial Cr (VI) Conc. (ppm)	ΔH(kJ mol^{-1})	ΔS (kJ mol^{-1} K^{-1})	ΔG (kJ mol^{-1})		
			293 K	313 K	333 K
15	−9.03	−0.02	−4.51	−4.20	−3.90
20	−13.75	−0.03	−5.82	−5.28	−4.74
25	−12.25	−0.02	−5.35	−4.88	−4.41

4. Conclusion

In this study, $BaTiO_3$ piezocatalytic nanoparticles were synthesized using the hydrothermal method. Temperature, time, and concentration were optimized. The synthesized nanoparticles were characterized using XRD, FE-SEM, TEM, Raman spectroscopy, and BET. It was found that, among the synthesized BaTiO3 nanoparticles, the one with highest removal percentage was synthesized at 200 °C for 13 h, which removed 96 % of 20 ppm Cr(VI). However, we studied the 200 °C and 10 h, which removed 92 %. This was to be able to study the effects of nanoparticle dosage, temperature, and concentration. The surface response methodology was used to optimize the removal temperature and concentration of Cr(VI). It was found that the optimum temperature and concentration were 20 °C and 17.32 ppm which removed 94 %. We have also studied the effect of adsorption on the removal of Cr(VI). It was found that only 15 % was removed by the adsorption on the surface of $BaTiO_3$, and 85 % was removed by pieozcatalytic reduction. Kinetic and thermodynamic properties of the reduction reaction were studied. It was found that the reaction was following the pseudo-first order. The results of thermodynamic studies suggest that at temperatures of 20 °C and concentrations of 20 ppm, the reaction was found to be most spontaneous. The activation energy was found to be 14.90 kJ/mol.

Funding information

This research did not receive any specific grant from funding agencies in the public, commercial, or not-for-profit sectors.

CRediT authorship contribution statement

Peshawa H. Mahmood: Writing – original draft, Methodology, Funding acquisition. **Omid Amiri:** Writing – review & editing, Supervision, Funding acquisition, Conceptualization. **S. Mohammad Sajadi:** Supervision.

Table 5
Comparison of different methods.

No.	Method	Conc. (ppm)	% Removal	Ref
1.	Bio adsorption (Escherichia coli and Bacillus subtilis) with zeolitic imidazolate framework-8	5	90 %	(Tang et al., 2022)
2	Photocatalyst (functionalized graphitic carbon nitride ($Cu_{3.21}Bi_{4.79}S_9/gC_3N_4$)	10	92.77 %	(Ajiboye et al., 2022)
3.	Anion Exchange Resin	15	98.20 %	(Leonard et al., 2023)
4.	Piezo–photocatalytic reduction (MoS2	8	96.2 %	(Li et al., 2023)
5.	Piezocatalysis (this work)	20	96 %	

Declaration of competing interest

The authors declare that they have no known competing financial interests or personal relationships that could have appeared to influence the work reported in this paper.

Data availability

Data will be made available on request.

Supplementary materials

Supplementary material associated with this article can be found, in the online version, at doi:10.1016/j.hazadv.2024.100468.

References

Ahamed, M., Akhtar, M.J., Khan, M.A.M., Alhadlaq, H.A., Alshamsan, A., 2020. Barium titanate (BaTiO3) nanoparticles exert cytotoxicity through oxidative stress in human lung carcinoma (A549) cells. Nanomaterials 10 (11), 2309. https://doi.org/10.3390/nano10112309.

Ahmed, S.S., Amiri, O., Rahman, K.M., Ismael, S.J., Rasul, N.S., Mohammad, D., Babakr, K.A., Abdulrahman, N.A., 2023. Studying the mechanism and kinetics of fuel desulfurization using CexOy/NiOx piezo-catalysts as a new low-temperature method. Sci. Rep. 13 (1), 7574. https://doi.org/10.1038/s41598-023-34329-y.

Ajiboye, T.O., Oyewo, O.A., Marzouki, R., Onwudiwe, D.C., 2022. Photocatalytic reduction of hexavalent chromium using Cu3.21Bi4.79S9/g-C3N4 nanocomposite. Catalysts 12 (10), 1075. https://doi.org/10.3390/catal12101075.

Almaguer-Busso, G., Velasco-Martínez, G., Carreño-Aguilera, G., Gutiérrez-Granados, S., Torres-Reyes, E., Alatorre-Ordaz, A., 2009. A comparative study of global hexavalent chromium removal by chemical and electrochemical processes. Electrochem. Commun. 11 (6), 1097–1100. https://doi.org/10.1016/j.elecom.2009.03.012.

Amiri, O., Abdulla, G.L., Burhan, C.M., Hussein, H.H., Azhdarpour, A.M., Saadat, M., Joshaghani, M., Mahmood, P.H., 2022. Boost piezocatalytic activity of BaSO4 by coupling it with BaTiO3, Cu:BaTiO3, Fe:BaTiO3, S:BaTiO3 and modify them by sucrose for water purification. Sci. Rep. 12 (1), 20792. https://doi.org/10.1038/s41598-022-24992-y.

Amiri, O., Ahmed, S.S., Younis, K.A., Rahman, K.M., Ismael, S.J., Rasul, N.S., Babakr, K. A., Abdulrahman, N.A., 2023. Pizo- catalytic desulfurization of model and real fuel samples over NiO/MnxOy nano-composite at room temperature: mechanism and kinetic behind it. Fuel 344, 128065. https://doi.org/10.1016/j.fuel.2023.128065.

Amiri, O., Beshkar, F., Ahmed, S.S., Hamad, B.W., Mahmood, P.H., Dezaye, A.A., 2021. Magnetically-driven Ag/Fe3O4/graphene ternary nanocomposite as efficient photocatalyst for desulfurization of thiophene under visible-light irradiation. Int. J. Hydrogen. Energy 46 (38), 19913–19925. https://doi.org/10.1016/j.ijhydene.2021.03.072.

Anah, L., Astrini, N., 2017. Influence of pH on Cr(VI) ions removal from aqueous solutions using carboxymethyl cellulose-based hydrogel as adsorbent. IOP Conf. Ser.: Earth Environ. Sci. 60, 012010 https://doi.org/10.1088/1755-1315/60/1/012010.

Asiaie, R., Zhu, W., Akbar, S.A., Dutta, P.K., 1996. Characterization of submicron particles of tetragonal $BaTiO_3$. Chem. Mater. 8 (1), 226–234. https://doi.org/10.1021/cm950327c.

Babakr, K.A., Amiri, O., Guo, L.J., Rashi, M.A., Mahmood, P.H., 2022. Kinetic and thermodynamic study in piezo degradation of methylene blue by SbSI/Sb2S3 nanocomposites stimulated by zirconium oxide balls. Sci. Rep. 12 (1), 15242. https://doi.org/10.1038/s41598-022-19552-3.

Brunauer, S., Emmett, P.H., Teller, E., 1938. Adsorption of gases in multimolecular layers. J. Am. Chem. Soc. 60 (2), 309–319. https://doi.org/10.1021/ja01269a023.

Chang, L.-Y., 2003. Alternative chromium reduction and heavy metal precipitation methods for industrial wastewater. Environ. Progress 22 (3), 174–182. https://doi.org/10.1002/ep.670220315.

Chaudhary, A.J., Goswami, N.C., Grimes, S.M., 2003. Electrolytic removal of hexavalent chromium from aqueous solutions. J. Chem. Technol. Biotechnol. 78 (8), 877–883. https://doi.org/10.1002/jctb.871.

Chen, H.-J., Chen, Y.-W., 2003. Hydrothermal synthesis of barium titanate. Ind. Eng. Chem. Res. 42 (3), 473–483. https://doi.org/10.1021/ie010796q.

Ciftci, E.; Rahaman, M.N.; Shumsky, M. Hydrothermal Precipitation and Characterization of Nanocrystalline BaTiO3 Particles. 8.

Deng, Y., Tang, L., Zeng, G., Zhu, Z., Yan, M., Zhou, Y., Wang, J., Liu, Y., Wang, J., 2017. Insight into highly efficient simultaneous photocatalytic removal of Cr(VI) and 2,4-diclorophenol under visible light irradiation by phosphorus doped porous ultrathin g-C3N4 nanosheets from aqueous media: performance and reaction mechanism. Appl. Catal. B: Environ. 203, 343–354. https://doi.org/10.1016/j.apcatb.2016.10.046.

Djellabi, R., Su, P., Elimian, E.A., Poliukhova, V., Nouacer, S., Abdelhafeez, I.A., Abderrahim, N., Aboagye, D., Andhalkar, V.V., Nabgan, W., Rtimi, S., Contreras, S., 2022. Advances in photocatalytic reduction of hexavalent chromium: from fundamental concepts to materials design and technology challenges. J. Water. Process. Eng. 50, 103301 https://doi.org/10.1016/j.jwpe.2022.103301.

El-Taweel, Y.A., Nassef, E.M., Elkheriany, I., Sayed, D., 2015. Removal of Cr(VI) ions from waste water by electrocoagulation using iron electrode. Egypt. J. Petrol. 24 (2), 183–192. https://doi.org/10.1016/j.ejpe.2015.05.011.

Gupta, V.K., Chandra, R., Tyagi, I., Verma, M., 2016. Removal of hexavalent chromium ions using CuO nanoparticles for water purification applications. J. Colloid. Interface Sci. 478, 54–62. https://doi.org/10.1016/j.jcis.2016.05.064.

Hayashi, H., Nakamura, T., Ebina, T., 2013. In-situ raman spectroscopy of BaTiO3 particles for tetragonal–cubic transformation. J. Phys. Chem. Solids 74 (7), 957–962. https://doi.org/10.1016/j.jpcs.2013.02.010.

Hong, K.-S., Xu, H., Konishi, H., Li, X., 2010. Direct water splitting through vibrating piezoelectric microfibers in water. J. Phys. Chem. Lett. 1 (6), 997–1002. https://doi.org/10.1021/jz100027t.

Huang, Y., Lee, X., Macazo, F.C., Grattieri, M., Cai, R., Minteer, S.D., 2018. Fast and efficient removal of chromium (VI) anionic species by a reusable chitosan-modified multi-walled carbon nanotube composite. Chem. Eng. J. 339, 259–267. https://doi.org/10.1016/j.cej.2018.01.133.

Ismael, S.J., Amiri, O., Ahmed, S.S., 2022. Preparation and characterization of La1−xMn1−yO3 piezocatalyst for removing waste drug pollutants in wastewater under the piezo-catalyst effect. Sep. Purif. Technol. 301, 121963 https://doi.org/10.1016/j.seppur.2022.121963.

Jadidi, M.; Etesami, N.; Esfahany, M.N. Adsorption and desorption processes of chromium ions using magnetic iron oxide nanoparticles and their relevant mechanism. 2017, 14 (3).

Kalhori, H., Amaechi, I.C., Youssef, A.H., Ruediger, A., Pignolet, A., 2023. Catalytic activity of $BaTiO_3$ nanoparticles for wastewater treatment: Piezo- or sono-driven? ACS Appl. Nano Mater 6 (3), 1686–1695. https://doi.org/10.1021/acsanm.2c04568.

Kant, T., Dahariya, N.S., Jain, V.K., Ambade, B., Shrivas, K., 2021. Chapter 18 - application of silver nanoparticles as a chemical sensor for detection of pesticides and metal ions in environmental samples. In: Abd-Elsalam, K.A. (Ed.), Silver Nanomaterials for Agri-Food Applications. Nanobiotechnology for Plant Protection; Elsevier, pp. 429–452. https://doi.org/10.1016/B978-0-12-823528-7.00030-5.

Khan, A., Toufiq, A.M., Tariq, F., Khan, Y., Hussain, R., Akhtar, N., Rahman, S.U., 2019. Influence of Fe doping on the structural, optical and thermal properties of α -MnO_2 nanowires. Mater. Res. Express 6 (6), 065043. https://doi.org/10.1088/2053-1591/ab0aaf.

Lace, A., Ryan, D., Bowkett, M., Cleary, J., 2019. Chromium monitoring in water by colorimetry using optimised 1,5-diphenylcarbazide method. IJERPH 16 (10), 1803. https://doi.org/10.3390/ijerph16101803.

Lakshmipathiraj, P., Bhaskar Raju, G., Raviatul Basariya, M., Parvathy, S., Prabhakar, S., 2008. Removal of Cr (VI) by electrochemical reduction. Sep. Purif. Technol. 60 (1), 96–102. https://doi.org/10.1016/j.seppur.2007.07.053.

Leonard, J., Sivalingam, S., Srinadh, R.V., Mishra, S., 2023. Efficient removal of hexavalent chromium ions from simulated wastewater by functionalized anion exchange resin: process optimization, isotherm and kinetic studies. Environ. Chem. Ecotoxicol. 5, 98–107. https://doi.org/10.1016/j.enceco.2023.03.001.

Li, X., Ren, Z., Zhang, Q., Guo, L., Wu, J., Li, Y., Liu, W., Li, P., Fu, Y., Ma, J., 2023. Piezo–photocatalytic reduction of toxic Cr(VI) ions based on MoS2 nanoflowers. Mater. Lett. 333, 133564 https://doi.org/10.1016/j.matlet.2022.133564.

Lin, E., Qin, N., Wu, J., Yuan, B., Kang, Z., Bao, D., 2020. $BaTiO_3$ nanosheets and caps grown on TiO_2 nanorod arrays as thin-film catalysts for piezocatalytic applications. ACS Appl. Mater. Interfaces 12 (12), 14005–14015. https://doi.org/10.1021/acsami.0c00962.

Masekela, D., Hintsho-Mbita, N.C., Sam, S., Yusuf, T.L., Mabuba, N., 2023. Application of BaTiO3-based catalysts for piezocatalytic, photocatalytic and piezo-photocatalytic degradation of organic pollutants and bacterial disinfection in wastewater: a comprehensive review. Arab. J. Chem. 16 (2), 104473 https://doi.org/10.1016/j.arabjc.2022.104473.

Maxim, F., Ferreira, P., Vilarinho, P.M., Reaney, I., 2008. Hydrothermal synthesis and crystal growth studies of $BaTiO_3$ using Ti nanotube precursors. Cryst. Growth Des. 8 (9), 3309–3315. https://doi.org/10.1021/cg800215r.

Meng, N., Liu, W., Jiang, R., Zhang, Y., Dunn, S., Wu, J., Yan, H., 2023. Fundamentals, advances and perspectives of piezocatalysis: a marriage of solid-state physics and catalytic chemistry. Prog. Mater. Sci. 138, 101161 https://doi.org/10.1016/j.pmatsci.2023.101161.

Motevalizadeh, L., Heidary, Z., Abrishami, M.E., 2014. Facile template-free hydrothermal synthesis and microstrain measurement of ZnO nanorods. Bull. Mater. Sci. 37 (3), 397–405. https://doi.org/10.1007/s12034-014-0676-z.

Moussout, H., Ahlafi, H., Aazza, M., Maghat, H., 2018. Critical of linear and nonlinear equations of pseudo-first order and pseudo-second order kinetic models. Karbala Int. J. Modern Sci. 4 (2), 244–254. https://doi.org/10.1016/j.kijoms.2018.04.001.

Nameni, M., Alavi Moghadam, M.R., Arami, M., 2008. Adsorption of hexavalent chromium from aqueous solutions by wheat bran. Int. J. Environ. Sci. Technol. 5 (2), 161–168. https://doi.org/10.1007/BF03326009.

Nassiri Mahallati, M., 2020. Advances in modeling saffron growth and development at different scales. Saffron. Elsevier, pp. 139–167. https://doi.org/10.1016/B978-0-12-818638-1.00009-5.

Navarro-Pardo, F., Martínez-Barrera, G., Martínez-Hernández, A., Castaño, V., Rivera-Armenta, J., Medellín-Rodríguez, F., Velasco-Santos, C., 2013. Effects on the thermo-mechanical and crystallinity properties of nylon 6,6 electrospun fibres reinforced with one dimensional (1D) and two dimensional (2D) carbon. Materials 6 (8), 3494–3513. https://doi.org/10.3390/ma6083494.

Owalude, S.O., Tella, A.C., 2016. Removal of hexavalent chromium from aqueous solutions by adsorption on modified groundnut hull. Beni. Suef. Univ. J. Basic Appl. Sci. 5 (4), 377–388. https://doi.org/10.1016/j.bjbas.2016.11.005.

Pakade E., V., Tavengwa T., N., Madikizela M., L., 2019. Recent advances in hexavalent chromium removal from aqueous solutions by adsorptive methods. RSC. Adv. 9 (45), 26142–26164. https://doi.org/10.1039/C9RA05188K.

Patel, K.S., Ambade, B., Jaiswal, N.K., Sharma, R., Patel, R.K., Blazhev, B., Bhattacharya, M.L., 2012. P. Arsenic and other heavy metal contamination in central India. In: Patel, K.S., Ambade, B., Jaiswal, N.K., Sharma, R., Patel, R.K., Blazhev, B. (Eds.), Understanding the Geological and Medical Interface of Arsenic - As 2012. CRC Press.

Pradhan, D., Sukla, L.B., Sawyer, M., Rahman, P.K.S.M, 2017. Recent bioreduction of hexavalent chromium in wastewater treatment: a review. J. Ind. Eng. Chem. 55, 1–20. https://doi.org/10.1016/j.jiec.2017.06.040.

Qin, G., McGuire, M.J., Blute, N.K., Seidel, C., Fong, L., 2005. Hexavalent chromium removal by reduction with ferrous sulfate, coagulation, and filtration: a pilot-scale study. Environ. Sci. Technol. 39 (16), 6321–6327. https://doi.org/10.1021/es050486p.

Qiu, B., Guo, J., Zhang, X., Sun, D., Gu, H., Wang, Q., Wang, H., Wang, X., Zhang, X., Weeks, B.L., Guo, Z., Wei, S., 2014. Polyethylenimine facilitated ethyl cellulose for hexavalent chromium removal with a wide pH range. ACS Appl. Mater. Interfaces 6 (22), 19816–19824. https://doi.org/10.1021/am505170j.

Rajapaksha, A.U., Selvasembian, R., Ashiq, A., Gunarathne, V., Ekanayake, A., Perera, V. O., Wijesekera, H., Mia, S., Ahmad, M., Vithanage, M., Ok, Y.S., 2022. A systematic review on adsorptive removal of hexavalent chromium from aqueous solutions: recent advances. Sci. Total Environ. 809, 152055 https://doi.org/10.1016/j.scitotenv.2021.152055.

Rengaraj, S., Yeon, K.-H., Moon, S.-H., 2001. Removal of chromium from water and wastewater by ion exchange resins. J. Hazard. Mater. 87 (1–3), 273–287. https://doi.org/10.1016/S0304-3894(01)00291-6.

Rouhaninezhad, A.A., Hojati, S., Masir, M.N., 2020. Adsorption of Cr (VI) onto micro- and nanoparticles of palygorskite in aqueous solutions: effects of pH and humic acid. Ecotoxicol. Environ. Saf. 206, 111247 https://doi.org/10.1016/j.ecoenv.2020.111247.

Saha, R., Nandi, R., Saha, B., 2011. Sources and toxicity of hexavalent chromium. J. Coord. Chem. 64 (10), 1782–1806. https://doi.org/10.1080/00958972.2011.583646.

Sedman, R.M., Beaumont, J., Mcdonald, T.A., Reynolds, S., Krowech, G., Howd, R., 2006. Review of the evidence regarding the carcinogenicity of hexavalent chromium in drinking water. J. Environ. Sci. Health, Part C 24 (1), 155–182. https://doi.org/10.1080/10590500600614337.

Shaukat, H., Ali, A., Bibi, S., Altabey, W.A., Noori, M., Kouritem, S.A., 2023. A review of the recent advances in piezoelectric materials, energy harvester structures, and their applications in analytical chemistry. Appl. Sci. 13 (3), 1300. https://doi.org/10.3390/app13031300.

Shiomi, S., 2023. Impurity-driven simultaneous size and crystallinity control of metal nanoparticles. Nanotechnology 34 (46), 465604. https://doi.org/10.1088/1361-6528/acf04c.

Tang, R., Shen, L., Yang, L., You, K., Li, Z., Wei, X., Wang, J., 2022. Killing two birds with one stone: biomineralized bacteria tolerate adverse environments and absorb hexavalent chromium. ACS Omega 7 (18), 15385–15395. https://doi.org/10.1021/acsomega.1c06877.

Tarjomannejad, A., Zonouz, P.R., Masoumi, M.E., Niaei, A., Farzi, A., 2018. LaFeO3 perovskites obtained from different methods for NO + CO reaction, modeling and optimization of synthesis process by response surface methodology. J. Inorg. Organomet. Polym. 28 (5), 2012–2022. https://doi.org/10.1007/s10904-018-0860-5.

Tu, S., Guo, Y., Zhang, Y., Hu, C., Zhang, T., Ma, T., Huang, H., 2020. Piezocatalysis and piezo-photocatalysis: catalysts classification and modification strategy, reaction mechanism, and practical application. Adv. Funct. Mater. 30 (48), 2005158 https://doi.org/10.1002/adfm.202005158.

Uchino, K., Sadanaga, E., Hirose, T., 1989. Dependence of the crystal structure on particle size in barium titanate. J. Am. Ceram. Soc. 72 (8), 1555–1558. https://doi.org/10.1111/j.1151-2916.1989.tb07706.x.

Vaiopoulou, E., Gikas, P., 2020. Regulations for chromium emissions to the aquatic environment in Europe and elsewhere. Chemosphere 254, 126876. https://doi.org/10.1016/j.chemosphere.2020.126876.

Verma, B., Balomajumder, C., 2020. Hexavalent chromium reduction from real electroplating wastewater by chemical precipitation. Bull. Chem. Soc. Ethiop. 34 (1), 67–74. https://doi.org/10.4314/bcse.v34i1.6.

Verma, R.L., Gunawardhana, L., Singh Kamyotra, J., Ambade, B., Kurwadkar, S., 2023. Air quality trends in coastal industrial clusters of Tamil Nadu, India: a comparison with major Indian cities. Environ. Adv. 13, 100412 https://doi.org/10.1016/j.envadv.2023.100412.

Wang, W., Cao, L., Liu, W., Su, G., Zhang, W., 2013. Low-temperature synthesis of BaTiO 3 powders by the sol–gel-hydrothermal method. Ceram. Int. 39 (6), 7127–7134. https://doi.org/10.1016/j.ceramint.2013.02.055.

Wei, Y., Zhang, Y., Geng, W., Su, H., Long, M., 2019. Efficient bifunctional piezocatalysis of Au/BiVO4 for simultaneous removal of 4-chlorophenol and Cr(VI) in water. Appl. Catal. B: Environ. 259, 118084 https://doi.org/10.1016/j.apcatb.2019.118084.

World Health Organization, 2020. Guidelines For Drinking-Water Quality (WHO-HEP-ECH-WSH-2020.3).

Xia, S., Song, Z., Jeyakumar, P., Shaheen, S.M., Rinklebe, J., Ok, Y.S., Bolan, N., Wang, H., 2019. A critical review on bioremediation technologies for Cr(VI)-contaminated soils and wastewater. Crit. Rev. Environ. Sci. Technol. 49 (12), 1027–1078. https://doi.org/10.1080/10643389.2018.1564526.

Xie, C., Niu, B., Guo, H., Ying, S., 2023. Piezoelectric-catalytic degradation of organic dyes and catalytic reduction of Cr(VI) with BaCO3@BaTiO3 microspheres. Inorg. Chem. Commun. 154, 110922 https://doi.org/10.1016/j.inoche.2023.110922.

Xu, H., Gao, L., Guo, J., 2002. Preparation and characterizations of tetragonal barium titanate powders by hydrothermal method. J. Eur. Ceram. Soc. 22 (7), 1163–1170. https://doi.org/10.1016/S0955-2219(01)00425-3.

Yuan, X., Li, J., Luo, L., Zhong, Z., Xie, X., 2023. Advances in sorptive removal of hexavalent chromium (Cr(VI)) in aqueous solutions using polymeric materials. Polym. (Basel) 15 (2), 388. https://doi.org/10.3390/polym15020388.